Long-term mercury accumulation and climate reconstruction of an Australian alpine lake during the late Quaternary

Margot Aurel Schneider [a,*], Larissa Schneider [a], Haidee Cadd [b], Zoë A. Thomas [c], Antonio Martinez-Cortizas [d], Simon Edward Connor [a], Georgia L. Stannard [e], Simon Graeme Haberle [a]

[a] School of Culture, History and Language. College of Asia and the Pacific, Australian National University, Canberra, ACT, Australia.
[b] ARC Centre of Excellence for Australian Biodiversity and Heritage, University of Wollongong, Wollongong, NSW, Australia
[c] School of Geography and Environmental Science, University of Southampton, Southampton, UK
[d] CRETUS, EcoPast, Facultade de Bioloxía, Universidade de Santiago de Compostela, Santiago de Compostela, Spain; and Bolin Centre for Climate Research, Stockholm University, Stockholm, Sweden
[e] Department of Archaeology and History, La Trobe University, Melbourne, Victoria, Australia

ARTICLE INFO

ABSTRACT

Mercury (Hg) is a volatile metal of international concern due to its toxicity, with a large atmospheric emission and transport capacity. The biogeochemical cycle of Hg is sensitive to changes in climate, yet our understanding of the specific impact of climatic factors on the Hg cycle remains limited. Here we use a multi-proxy framework, supported by AMS ^{14}C dating, to interpret climatic events in South-Eastern Australia from ~18,000 years to 6500 years before present from the sediments of Blue Lake in Australia's alpine region. By combining Hg analysis with Antarctic temperature records and iTRACE climate model outputs, carbon-to-nitrogen ratios (C:N), macroscopic charcoal, and pollen analysis, we find Hg records within Blue Lake's sediments primarily reflect changes in the catchment as a result of a changing climate. The increase in Hg concentrations began with the onset of the Holocene, following a glacial period during which the region was predominantly rocky, relatively barren, and likely covered by ice and snow. The strong relationship between Hg and organic matter in our record indicates that soil development in the watershed post de-glaciation was a predominant driver of Hg concentration and deposition in Blue Lake. An increase in precipitation and temperature in the Holocene contributed to an increase in nutrients and organic matter, further increasing Hg concentration in Blue Lake. A primary challenge in modern Hg research, particularly in the context of climate change, involves distinguishing changes in Hg levels resulting from human activities from those driven by climatic variations. Our pre-anthropogenic data highlight the long-term interrelationships among climate dynamics, soil processes, and ecological transformations within lake catchments on the geochemical cycle of Hg. These connections should be factored into strategies aimed at mitigating Hg increases in lake sediments resulting from global warming.

1. Introduction

Mercury (Hg), a toxic metal of global concern, exhibits heightened sensitivity to climatic fluctuations owing to its pronounced volatility (Lin and Pehkonen, 1999). This characteristic facilitates its widespread dispersion in the environment, primarily through atmospheric emissions and subsequent transport, making its behaviour and impact an issue of global environmental significance (Beckers and Rinklebe, 2017; Obrist et al., 2018). It is released into the environment as a result of human activities and natural processes such as volcanoes and rock weathering (Fitzgerald and Lamborg, 2005; Swartzendruber and Jaffe, 2012). Following its release, Hg is transported and recycled among environmental compartments until it is removed from the surface system through deposition in sediments (Fitzgerald et al., 2018; Outridge et al.,

2018).

In an effort to mitigate global Hg emissions, the Minamata Convention on Mercury, an international treaty developed under the auspices of the United Nations, was established in 2013 (Kessler, 2013). The treaty became effective in August 2017, and since its implementation, the United Nations Environment Programme (UNEP) has committed to conducting comprehensive assessments of the scientific literature pertaining to Hg every five years (UNEP, 2018). One focus of these discussions is the understanding of the effects of climate change on the biogeochemical cycling of Hg. This knowledge is instrumental in enhancing our predictive capabilities regarding the impacts of contemporary global warming on Hg emissions across various environmental matrices, as well as its consequent exposure to biota and human populations.

Considering the extended time scales over which natural climate changes occur and the anthropogenic emissions of Hg, directly correlating contemporary shifts to impacts on the Hg cycle presents significant challenges. Paleolimnology (the study of lake sediments) and its associated methods are powerful tools that can support the study of climate effects on the Hg cycle (Cooke et al., 2020). Lake sediments serve as repositories for environmental proxies and Hg deposition, thus providing a historical record of atmospheric Hg accumulation rates (Hg$_{AR}$) (Thomas et al., 2022), while also facilitating the indirect reconstruction of past climatic and environmental changes (Hermanns and Biester, 2013; Saunders et al., 2018).

In the last 20 years, studies have consistently demonstrated that Hg concentrations and fluxes in the deposition of lake sediments in the Southern Hemisphere have increased by at least fourfold since the onset of the Industrial Revolution, primarily due to a rise in anthropogenic emissions (Lamborg et al., 2002; Lindberg et al., 2007; Engstrom et al., 2014; Li et al., 2020; Cooke et al., 2022). Modern global warming represents an additional concern, as it is associated with further increases in Hg deposition (Schneider et al., 2020; Thomas et al., 2022). However, there remains a notable paucity of comprehensive research elucidating the specific mechanisms by which climate change may exacerbate Hg emissions, as well as the geographical variability of these processes on a global scale.

The period between the end of the Last Glacial Maximum (LGM) and the start of the Holocene (~20, 000–11,700 calibrated years before present; cal BP) was marked by rapid global climate (warm and cold) oscillations (Williams et al., 2009). These rapid climatic oscillations are ideal periods to investigate how ecological and geochemical processes alter the atmospheric cycling of Hg and its deposition in terrestrial and aquatic environments. During the transition from the LGM and into the start of the Holocene (approximately 14,500 to 11,500 cal BP), the globe experienced rapid warming followed by cooling (Kaufman and Broadman, 2023), including the notable Southern Hemisphere (SH) cooling of the Antarctic Cold Reversal, which is known to have been a period of cooling in the Australian Alps bioregion (ACR; Pedro et al., 2016).

The LGM and subsequent deglacial period and the associated mechanistic understanding of these climatic oscillations are mostly confined to the Northern Hemisphere (Petherick et al., 2022). The magnitude, timing, and mechanisms of climate oscillations in the SH are debated, though studies suggest that they are potentially triggered by perturbations of the Atlantic thermohaline circulation. The Australian Alps bioregion is located within the southern westerly wind (SWW) belt and is influenced by El Niño-Southern Oscillation (ENSO). It is the only area on the Australian mainland where glaciation during the LGM has been confirmed (Barrows et al., 2001), followed by climate amelioration after ~18,000 cal BP (Cadd et al., 2021; Cadd et al., 2024), and estimated to have become completely deglaciated by 15,800 cal BP (Williams et al., 2009). This intense change in climate makes the region ideal for studying the effects that climate has on the Hg cycle in Australia.

This study aimed to increase our understanding of long-term climate change in the SH using mercury as a climate proxy. We examined a 2-m-long segment of lake sediment core (from 400 to 613 cm) from Blue Lake, a glacial lake in the Australian Alps bioregion. We focus on this climatologically dynamic time period to explore long-term drivers of change in atmospheric Hg deposition and catchment dynamics. By comparing our Hg record with modelled temperature records in the Australian Alps bioregion and Antarctica, as well as a range of ecological proxies, including pollen, charcoal, organic matter content, and the carbon to nitrogen ratio (C:N), we reconstruct environmental, ecosystem, and Hg responses to climate changes during the late Pleistocene and early Holocene. It is hypothesised that these proxies will emphasise ecological changes associated with vegetation and fire activity linked to climatic variability, allowing us to understand how the climate of this period in the Australian Alpine bioregion impacted the Hg cycle.

2. Methods

2.1. Study Location

Blue Lake is a freshwater lake in the Australian Alps bioregion, approximately 400 km southwest of Sydney in Australia's Alpine region (36.404314° S, 148.315372° E, Fig. 1). During the Last Glacial Maximum (LGM), the alpine region underwent glaciation (Barrows et al., 2001), with Blue Lake emerging as the sole Australian mainland lake carved by glacial erosion and subsequent melting processes (David et al., 1901; Dulhunty, 1945; De Deckker et al., 2023). It is located at 1930 m above sea level (a.s.l.), approximately 5 km from Mount Kosciuszko, Australia's highest mainland peak at 2228 m a.s.l. The Australian Alpine bioregion experiences an average annual precipitation of approximately 1770 mm yr^{-1}, with temperatures ranging from 16.9 to −5.2° C, resulting in a mean annual temperature of 4.2 ° C, (De Deckker et al., 2023), with snow/snow patches present for an average of >245 days of the year (Green and Pickering, 2009).

Blue Lake has a maximum water depth of 28 m and occupies an area of 16 ha, with a length of 540 m and a width of 360 m (Fig. 1). It has a relatively small catchment area of 1.9 km^2 (De Deckker et al., 2023) in proportion to the lake area (catchment to lake ratio = 11.8). Previously Blue Lake has been assumed to have become deglaciated at approximately 15,800 cal BP (Williams et al., 2009). Currently the area experiences freezing conditions during the winter season, rendering it the sole dimictic lake on the Australian mainland (Raine, 1982).

Blue Lake was strategically chosen for evaluating mercury (Hg) responses to climate variations during the Last Glacial Maximum (LGM) for several reasons. It is remote and sparsely populated location minimises human influence; being an isolated lake without connections to extensive aquatic systems reduces potential sediment disturbance and input of material from external water courses (Vernon, 2017). Situated at the highest point in Australia, its location renders it highly responsive to climate variations. Being a glacial lake, Blue Lake is expected to capture changes in glacier size, extent, and dynamics resulting from climate shifts within its sedimentary layers (Stansell et al., 2013).

The vegetation surrounding Blue Lake consists predominantly of heath and alpine daisy species, with sparse occurrences of the mountain plum-pine (*Podocarpus lawrencei*), forming what is known as the Tall Alpine Herb Field plant community (Costin et al., 1979). Blue Lake is located above the current tree line, occurring within the altitudinal range of 1800 and 1900 m (Auld et al., 2022). During the LGM, the lower temperatures and CO$_2$ concentrations (Sigman and Boyle, 2000; Menviel et al., 2018; Du et al., 2023; Cadd et al., 2024) likely would have inhibited tree and shrub growth within the Blue Lake catchment and resulted in a substantially lower tree line than the present day (Raine, 1974; De Deckker et al., 2020; De Deckker et al., 2023).

The main geological units in the Blue Lake catchment are Carboniferous granites and Ordovician metasediments. The regolith is thin and is comprised of weathered granites and metamorphosed shales in addition to shallow organic-rich soils (De Deckker et al., 2023). Soils consist of silty clays which were found to erode easily in summer rain,
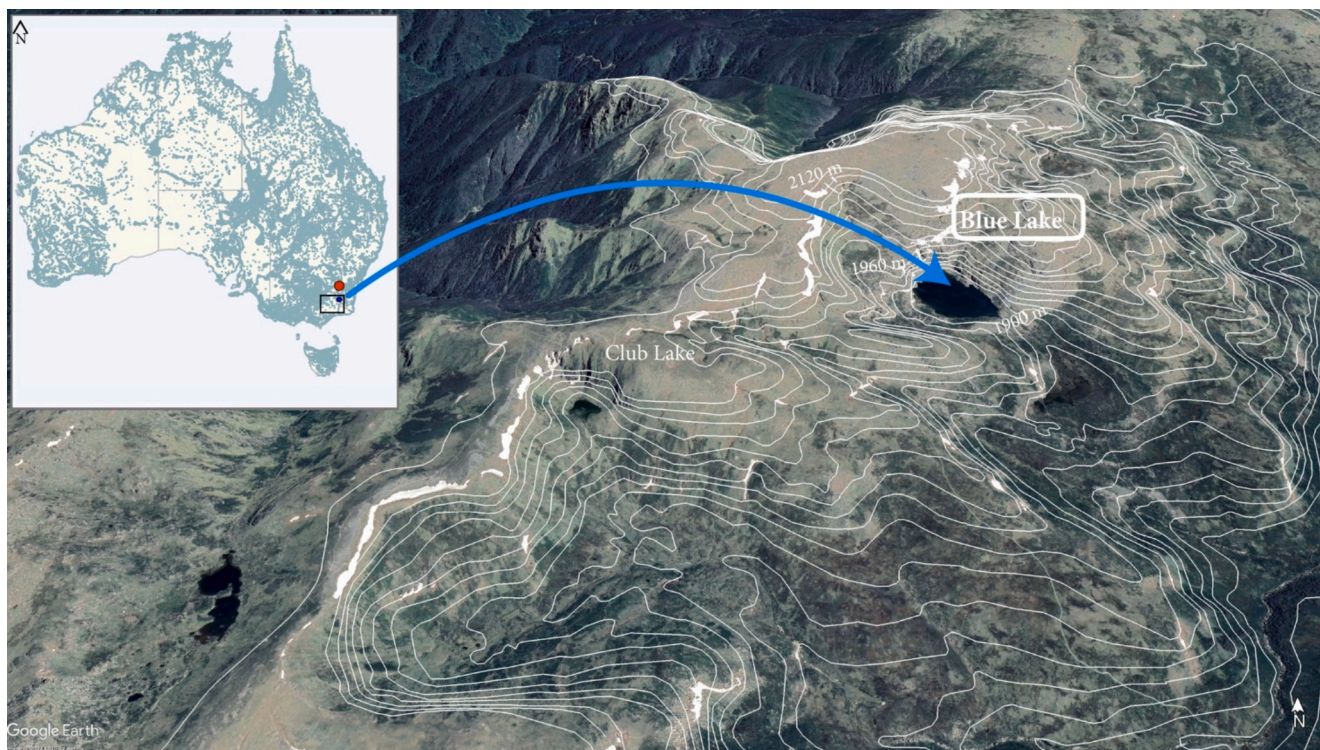
Fig. 1. Location of Blue Lake, southeast Australia, in the state of New South Wales, satellite image of Blue Lake with contours every 15 m (Google Earth) with the adjacent Club Lake (Thomas et al., 2022) The inset provides an overview of the location of Blue Lake in Australia, Canberra is indicated with a red circle, and Blue Lake is indicated by a dark blue dot. Light blue on the map of Australia indicates water sources in Australia. The black rectangle in South-Eastern Australia represents the bounds for the iTRACE temperature model. (For interpretation of the references to colour in this figure legend, the reader is referred to the web version of this article.)

and stable, organic-rich peaty-clays under the herb field community (Costin et al., 1979).

2.2. Sediment sample collection

The core was collected using a Mackereth corer (Mackereth, 1958; Smith, 1959) from the deepest point of Blue Lake (28 m), and sub-sampled in 2006. This 6 m core was capped, sealed, and transported to the Australian National University (ANU) for storage and analysis. Subsequently, the core was sliced at 1 cm intervals and stored in a coolroom at 4 °C within the Archaeology and Natural History facilities in the School of Culture, History & Language.

This study's primary emphasis was on the analysis of the 400 to 613 cm section of the core, as this interval encompasses the critical transition period between the LGM and the Holocene. The sediments in this section of the core were light in colour and largely inorganic, reflecting the high altitudinal nature of the lake, and the weathered granites and meta-morphosed shales present in the catchment.

2.3. Sample analysis

Before undergoing analyses, 15 mL of sediment sample was weighed while still wet. Subsequently, they underwent a freeze-drying process for 72 h using a Christ Alpha 1–2 LDplus lyophilizer (John Morris Scientific, Sydney, Australia). After the drying process, the samples were reweighed to measure dry bulk density (weight divided by volume). Following this, the samples were divided for further analyses as outlined below:

2.4. Radiocarbon dating and age modelling

Bulk sediment samples were processed for analysis of radiocarbon

(^{14}C). Five initial ages were obtained by accelerator mass spectrometry at DirectAMS (Washington, USA) and then ten samples at the Chronos Radiocarbon Facility, UNSW (Sydney, Australia) to further constrain the chronology.

The dried, crushed samples were pre-treated with an acid-base-acid method to remove carbonates and humic and fulvic acids and washed with milli-Q water (Turney et al., 2021). The insoluble residue was freeze-dried for AMS analysis.

A Bayesian age model was constructed in OxCal 4.4 from the radiocarbon age determinations using a 'P_sequence deposition model' (Bronk Ramsey, 2008; Ramsey and Lee, 2013) with the 'general outlier' analysis detection method (probability = 0.05) (Ramsey, 2009). The radiocarbon ages were converted into calendar years using the SHCal20 calibration curve (Hogg et al., 2020). The model uses Bayesian statistics to quantify the most likely posterior age distributions using the proba-bility density from radiocarbon calibration and the stratigraphic order of the sequence, to provide a robust age model.

2.5. C:N analysis

Carbon (C) and nitrogen (N) analyses were undertaken at the Mark Wainwright Analytical Centre Solid State and Elemental Analysis XRF Laboratory at UNSW. A total of 43 samples were measured, along with four measurements of sulfamethazine as the certified reference stan-dard, on the Elementar varioMACRO cube. Results from the standard reference material are given in Supplementary Table 1. The lower detection limit of this method is 0.08% and 0.27% for N and C, respectively, providing 30 mg sample weight. Concentration values below the calibration range may be less accurate.

2.6. Total Organic Matter

Before conducting this analysis, concentrated HCl (37% HCl Merck Suprapur, Germany) was added to five samples as a preliminary step to assess the presence of carbonates. Since no observable reaction occurred upon the introduction of HCl, we proceeded with the organic C analyses on 132 samples without the need for HCl pre-treatment.

Total organic matter (OM) analyses were performed using the weight-loss-on-ignition method described by Wang et al. (2011). Samples were sieved (< 2 mm) and 1000 ± 200 mg of each sample was weighed out and heated in a muffle furnace (model CEMLL-SD; Labec, Sydney, Australia) at $550°$ for six hours. Once cooled to room temperature, samples were weighed, and the difference was reported as organic content mass percentages. Total OM analysis was conducted on most samples used for Hg analysis.

2.7. Mercury analyses

Mercury analyses were conducted using a Milestone Direct Mercury Analyzer (DMA-80 Tri-Cell; Milestone, Bergamo, Italy), calibrated with aqueous Hg standard for AAS Sigma Aldrich TraceCERT® (1000 mg/L Hg in nitric acid). The lower detection limit for the DMA-80 is 0.01 ng of Hg. A total of 133 samples were selected for Hg analysis, the first 50 cm were analysed at a 1-cm resolution to provide a high-resolution record in the early Holocene, followed by every second cm for the remainder of the core.

A calibration curve was constructed by plotting the absorbances of standards in nanograms against Hg concentrations, which was considered valid for an R^2 value of 0.99 or higher.

The DMA-80 determines total Hg concentration through thermal decomposition, amalgamation, and atomic absorption spectrometry. Samples were analysed using the USEPA method 7473 (USEPA (US Environmental Protection Agency) 1998): two blanks and two Standard Reference Materials (SRMs) were analysed for every 40 samples. Approximately 100 mg of sample was weighed in nickel boats and, every tenth sample, a replicate sample was analysed. When replicate recovery exceeded 10% compared to the original sample, a third replicate was run. Certified sediment reference materials NIST-2711a (Montana River Sediment) and SECCC WQB-1 (Lake Ontario) were analysed, and results were in agreement with published values (Supplementary Table 2).

2.8. Mercury Accumulation Rate

Mercury accumulation rate (Hg_{AR}, ng m^{-2} y^{-1}) in this study was calculated following equation:

$$HgAR = (SR*DBD*Hg)*10$$

where SR = sedimentation rate (cm yr^{-1}); DBD = dry bulk density (g cm^{-3}); Hg = Hg concentration (ng g^{-1}). The factor of 10 is applied for unit conversion purposes.

2.9. Macro Charcoal

Charcoal particles are an indicator of fire occurrence, with macroscopic particles considered indicative of catchment-scale fires and microscopic particles representative of broader regional-scale burning patterns (Long et al., 2021). Microscopic charcoal (30 samples) was quantified alongside pollen and non-pollen palynomorphs by counting opaque black particles 10 to 100 μm in size. Every cm of the core, apart from one sample (at 612 cm), was analysed for contiguous macroscopic charcoal (a total of 212 samples). Samples were sieved at two size fractions (125 μm and 250 μm) from a known volume of sediment. Particles were identified using a binocular microscope. All macroscopic charcoal results were combined into a total charcoal count for analysis. The charcoal accumulation rate (CHAR, in cm^2 yr^{-1}) was calculated as the ratio of charcoal concentration (particles cm^3) to the accumulation rate (sedimentation rate in cm yr^{-1}).

2.10. Pollen

A total of 30 samples, evenly spaced throughout the core, were prepared for pollen, spores and microcharcoal identification using a modified version of Faegri et al. (1989). Dried sediment samples were treated with 10% potassium hydroxide at $80°°C$ for 20 min prior to sieving through a 100 μm mesh sieve. Sieving was followed by the addition of a single *Lycopodium* spore tablet and 10% hydrochloric acid. Silicates were separated using sodium polytungstate heavy liquid separation with a specific gravity of 1.9–2.0. Float material was then subject to acetolysis treatment, being heated in a 9:1 mixture of acetic anhydride and sulfuric acid, before samples were mounted in glycerol and sealed with nail varnish. Identification and counting of pollen, microscopic charcoal and spores was undertaken on a light microscope at x 400 magnification.

Pollen samples were counted until a total of 300 pollen grains of terrestrial origin were identified. The terrestrial pollen count forms the base pollen sum while percentages of aquatic taxa include a sum of both aquatic and terrestrial pollen taxa. A combined sum of all taxa forms the basis for percentages of algal species. Concentration data of pollen and microcharcoal counts was calculated for all pollen taxa using counts of exotic marker grains of *Lycopodium*, sediment subsample volume and pollen counts.

2.11. Modelled temperature

Proxy data was compared to modelled temperature outputs from the iTRACE transient climate experiment that simulates global, long-term millennial-scale climate evolution across the terminal Last Glacial Maximum (LGM) and post glacial period, utilising the Community Earth System Model (CESM) version 1.3. (Brady et al., 2019; He et al., 2021b). Simulated temperature estimates represent the radiative surface temperature (TS; degree Celsius; $°C$) from 20,000 to 11,000 cal BP at a resolution of 1.9° in latitude and 2.5° in longitude (He et al., 2021a). The decadal averaged surface temperature output for the grid cell containing Blue Lake was extracted and compared to proxy outputs.

2.12. Statistical Analysis

We conducted all analyses in RStudio Version (2023.06.1 + 524) (R Core Team, 2020). The 'ggplot2' package (Wickham and Chang, 2016) was used to visualise environmental and geochemical proxies in Blue Lake. The 'ggpubr' package was used to perform Pearson correlations, using the function 'ggscatter' for visualisations (Kassambara and Kassambara, 2020). The 'vegan' package (Oksanen et al., 2007) was used to perform both principal component analysis (PCA) and detrended correspondence analysis (DCA). A DCA was run on square-root transformed terrestrial taxa (pollen data) to account for non-linear ecological responses to environmental variables. The DCA scores represent ecological turnover and can therefore be interpreted as change in plant community composition. Pollen taxa most highly correlated with the DCA axes were identified to assist with the ecological interpretation. To compare the pollen ordination to the higher resolution geochemical ordination, we interpolated DCA axis 1 scores and plotted them by age. These interpolated DCA scores were then incorporated as a variable into a PCA alongside climate proxies. The climate proxies (log-transformed) included in the PCA were: Antarctic temperature ($+10°C$ to account for negative values in the temperature data for log transformation) (Parrenin et al. 2013), C:N, CHAR, OM%. The C:N analysis was conducted at the lowest resolution and due to N values below 574 cm being below the lower detection limit, the C:N values below this depth were removed. Therefore, the PCA represents data from 17,838 to 6750 cal BP. To understand how Hg_{AR} relates to the other environmental variables, Hg_{AR}

was passively plotted with the function 'ordisurf' in the 'vegan' package. The 'ordisurf' function plotted Hg_{AR} using a generalised additive model (GAM), predicting Hg_{AR} as a function of the other variables in the ordination (Oksanen, 2015).

3. Results and Discussion

3.1. Core Chronology and Sedimentology

The ^{14}C age-depth model from 15 samples for Blue Lake on bulk sediment (Supplementary Table 3) revealed increasing age with depth, with no evidence for post depositional mixing of sediments (Fig. 2). There were two outliers at 510 cm and 610 cm, with both samples dated as younger than the surrounding sediments. These were excluded from the age model. The median modelled ages from the bulk sediments spanned from 20,210 to 6750 cal BP, corresponding to the late Pleistocene and early Holocene. Unfortunately, no samples deeper than 574 cm had sufficient C (C content <2%) for radiocarbon dating (> 4%). Therefore, the age model was extrapolated from 574 cm (17,838 cal BP) to the base of the core at 613 cm. Due to the inherent uncertainties and
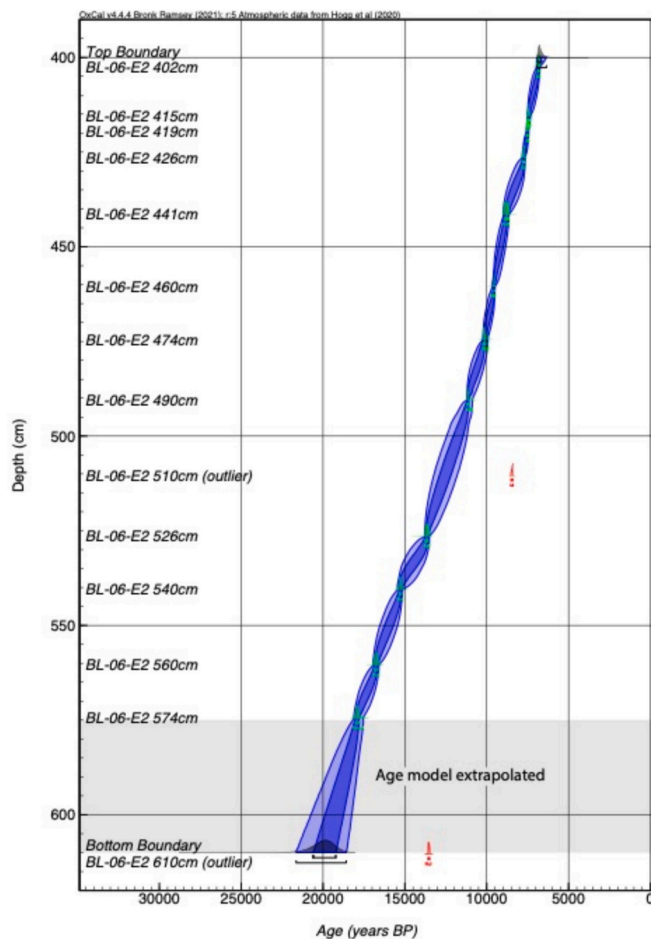
Fig. 2. Age-depth model for Blue Lake sediments using a P_sequence deposition model in OxCal 4.4 (Bronk Ramsey, 2008; Bronk Ramsey and Lee, 2013). 1σ and 2σ age ranges (dark and light blue envelopes respectively) and probability distributions generated from the Bayesian age model are shown. Two samples outside the 1σ and 2σ age ranges denote outliers that were excluded from the age model. The ^{14}C ages were calibrated against the Southern Hemisphere calibration (SHCal20) data set (Hogg et al., 2020). The grey shaded 610 cm histogram represents an extrapolated age probability distribution function for the base, with ages extrapolated between the depths of 574 to 613 cm. (For interpretation of the references to colour in this figure legend, the reader is referred to the web version of this article.)

the likelihood that the sedimentation rate would have slowed considerably, the base of the core is interpreted to be approximately 18,000 years old (Supplementary Table 3).

The age-depth model suggests a mean sedimentation rate for this section of the core (400 to 613 cm) of 0.017 cm/yr (± 0.006, Figs. 2 and 3). However, there is high uncertainty in the sedimentation rate for the lowermost section of the core (sedimentation rate 0.016 cm/yr between 609 and 575 cm) due to the extrapolated age-depth model from 575 cm to base. Data which directly uses sedimentation rate to calculate flux include Hg_{AR} and CHAR, and are therefore likely to have large uncertainties at this depth (Fig. 3). The sedimentation rate decreases to an average of 0.013 cm/yr between 574 cm and 541 cm (modelled at 17,838 and 15,312 cal BP), then decreasing to 0.009 cm/yr between 540 and 527 cm (modelled at 15,000 to 13,720 cal BP). It then increases again to an average of 0.014 cm/ yr between 527 and 473 cm (modelled at 13,720 to 10,063 cal BP). Sedimentation increases further to 0.025 cm/yr between 472 and 442 cm (modelled at 10,002 and 8819 cal BP), followed by a further increase to an average of 0.034 cm/yr from 426 to 415 cm (modelled at 7720 to 7399 cal BP) before declining again at the top of the core (Figs. 2 and 3).

Sediment throughout the core was composed of fine inorganic material. Previous studies on Blue Lake which have included grain size analyses, have identified most of the sediment particles to be <200 μm, and when viewed under the electron microscope, rhomboid calcite crystals were present (Leaney et al., 1995).

3.2. Climate and Ecological Changes

3.2.1. Pleistocene termination (~18,000 to 15,000 cal BP – 613 to 539 cm)

The data related to pollen, climate and ecological proxies, including organic matter, charcoal, and C:N ratio, are summarised in Fig. 3, as well as Supplementary Table 5, and Supplementary Fig. 1. From the base of the core to 15,000 cal BP, the pollen composition of Blue Lake features high values of Asteraceae and Poaceae, and the highest values in the sequence of *Leptospermum/Baeckea*, Ranunculaceae and *Plantago*, indicative of an alpine heath and herbfield vegetation community, with lower pollen accumulation rates (Fig. 3, Supplementary Fig. 1). This vegetation composition, and low pollen accumulation (Supplementary Fig. 1) indicates a low productivity environment with limited vegetation cover, likely due to colder and potentially drier climates and low CO_2 levels (Sigman and Boyle, 2000; Menviel et al., 2018; Du et al., 2023; Cadd et al., 2024). Additionally, this section of the core showed the lowest OM percentages (Fig. 3). These lower OM contents are aligned with the lowest temperatures (Fig. 3) during this study's timeframe.

The abundance (30–40%) of wind-borne, long-distance travelled pollen such as *Casuarina* and Amaranthaceae, which were unlikely to be growing within the catchment (Fig. 3, Supplementary Fig. 1) further supports the interpretation of a sparsely vegetated or largely unvegetated catchment. The abundance of these over-represented lowland taxa (Mariani et al., 2018) may suggest the presence of strong winds (De Deckker et al., 2019).

The C:N ratios measured at the base of the core, until 17,838 cal BP, had N levels significantly below the lower detection limit, and no interpretation was drawn from these samples. The C:N ratio from 17,838 to 15,000 increases along with temperature, OM and the pollen accumulation rate (PAR, Fig. 3 and Supplementary Fig. 1). The far-travelled pollen also begins to decline (Fig. 3). This increase in C:N could therefore be attributed to an increase in OM from the catchment (Kaushal and Binford, 1999).

Fire activity, indicated by charcoal accumulation rate (CHAR), remains relatively low at the lowermost depths, consistent with the relative lack of vegetation biomass during the early deglacial period. Fire activity increases at 17,838, concurrent with increases in Antarctic and modelled temperature (Fig. 3). A further abrupt increase in both CHAR and charcoal counts occurs between 16,000 and 15,000 cal BP (Fig. 3),
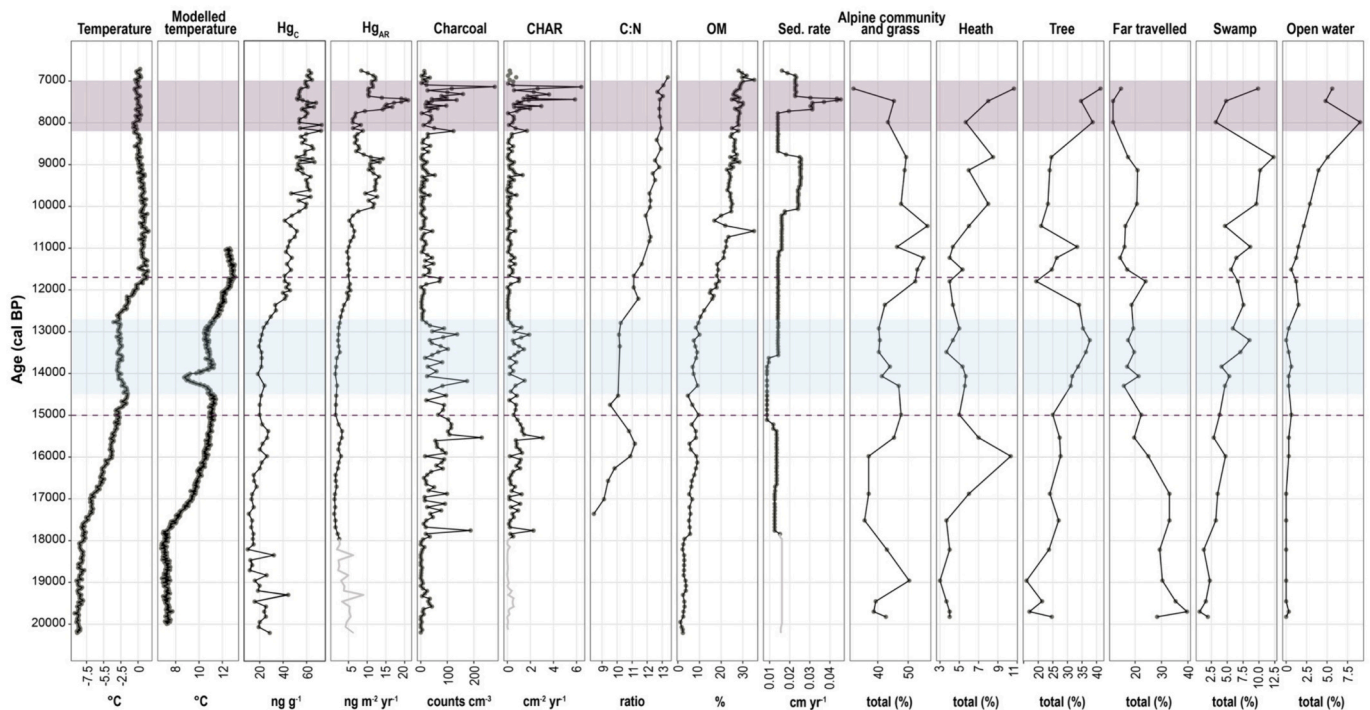
Fig. 3. Stratigraphic diagram of Temperature = reconstructed Antarctic temperature Parrenin et al., (2013), Modelled temperature = °C modelled surface temperature of the Blue Lake region, mercury (Hg) concentration (ng g^{-1}), Hg accumulation rate (ng m^{-2} y^{-1}), Charcoal = macroscopic charcoal concentration, CHAR = macroscopic charcoal accumulation rate, C:N = carbon to nitrogen ratio, OM = organic matter, Sed.rate = sedimentation rate, Alpine plant community and grass pollen, Heath pollen, Tree pollen, Far travelled pollen, Swamp pollen, and open water pollen. For a list of species included in these community level pollen totals, see supplementary Table 4. Solid black lines indicate trend in the data, grey points indicate measured values. Grey lines indicate uncertainty in the data associated with extrapolated age depth model and sedimentation rate to calculate these values. C:N data at the bottom of the core was removed due to N values falling well below the lower detection limit of the method. Purple dotted lines indicate time period distinction, 15,000 cal BP denotes the end of the Pleistocene termination and beginning of the Holocene transition, the 11,700 cal BP line indicates the beginning of the Early Holocene. The Blue shaded section from 14,500 to 12,700 cal BP = Antarctic cold reversal (Cadd et al., 2024) and the purple shaded section from 7000 to 8200 cal BP indicates a previously known warm period in south-eastern Australia (De Deckker, 2022) (For interpretation of the references to colour in this figure legend, the reader is referred to the web version of this article.)

potentially indicating a shift in vegetation communities and temperature towards the end of the Pleistocene Termination (Fig. 3).

3.3. Holocene transition (~15,000 to 11,700 cal BP; 538 to 499 cm)

The pollen results during the transition to the Holocene in Blue Lake, particularly the increase in tree pollen, suggest this to be a period gradually shifting towards a warmer and potentially wetter climate (Fig. 3). Both Antarctic ice-core derived temperature reconstructions and iTRACE modelled temperature records show rapidly increasing temperatures from ~18,000 cal BP until the onset of the Antarctic Cold Reversal (ACR) at 14,500 cal BP (Pedro et al., 2016). The ACR is characterised by a protracted decline in the Antarctic temperature stack from 14,500 to 12,800 cal BP (Parrenin et al. 2013), while the modelled temperature from the Blue Lake region indicates a rapid ~2 °C decrease in temperatures between 14,400 and 13,900 cal BP (Fig. 3). There is a slight decrease in the PAR (Supplementary Fig. 1) during this time period; however, this is short-lived and is not maintained for the entire period of cooling suggested by the Antarctic temperature record (Fig. 3, Parrenin et al. 2013). This could indicate that the ACR in the Australian Alps bioregion was shorter in duration than in Antarctica (Fig. 3, (Parrenin et al., 2013), consistent with the iTRACE temperature output (Fig. 3) (Williams et al., 2009; Pedro et al., 2016; Cadd et al., 2024).

The pollen record shows a shift from heath-dominated vegetation to tree-dominated and, following the period of cooling, indicates an increase in the altitude of the tree line, likely driven by increases in temperature and rainfall (Fig. 3). Swamp-adapted vegetation increases concurrently, with increases in the presence of *Gonocarpus, Haloragis*, Restionaceae, *Epacris*, and fern spores (Fig. 3 and Supplementary Fig. 1).

The increased presence of alpine bog and fern taxa, particularly from Restionaceae, *Haloragis* and *Gonocarpus* species, which are known to thrive in waterlogged soils (Orchard, 1979; Linder et al., 1998), is an additional indication of a transition towards a warmer and wetter climate (Fig. 3; Supplementary Fig. 1). Between 14,500 to 12,800 cal BP, CHAR levels fluctuate, potentially indicating a variable climate and the transition towards higher biomass tree-dominated vegetation. This hypothesis is reinforced by charcoal data in previous studies, which have shown that increases in charcoal accumulation often accompany transitional periods in climate or vegetation (Kershaw et al., 2002).

Additionally, the monolete and trilete spores found in the sediment (Supplementary Fig. 1) are likely associated with *Sphagnum* moss, ferns and fern allies, requiring warmer environments and high humidity to grow (Kessler and Kluge, 2022). Organic matter between 14,500 and 12,800 cal BP remains relatively stable, yet from 12,800 cal BP, this also begins to increase (Fig. 3). These findings potentially suggest an increase in water availability from 12,800 cal BP, possibly influenced by an increase in temperature. The C:N ratios are relatively stable between 15,000 cal BP to 12,800, suggesting limited catchment disturbance and lake productivity during this period (Devesa-Rey and Barral, 2012).

3.3.1. The Early Holocene (~11,700 to 6750 cal BP; 498 to 400 cm)

The early Holocene is a period of major vegetation change in Blue Lake. The pollen record shows an increase in montane forest species with an increase in *Eucalyptus dalrympleana*-type, *E. viminalis*-type, *Epacris*, Laminaceae, Rhamnaceae (*Pomaderris*), Apiaceae, *Coprosma*, and *Dodonaea* (Fig. 3 and Supplementary Fig. 1). While not reflected in the Antarctic temperature reconstruction (Fig. 3), the increase in arboreal taxa suggests a rise in moisture and temperature levels in the region

([Martin, 1999](#)), indicating an expansion of the tree line upslope and a potentially local presence of montane forest with a shrub understory.

The warming trend for this period is further evidenced in the increased presence of open-water species like *Botryococcus* green algae ([Fig. 3](#) and Supplementary Fig. 1). These species could indicate a reduction in ice cover over the lake and warmer water temperatures (particularly in summer), supporting the growth of these algal species.

Between 12,500 and 8200 cal BP, we observe consistent yet small values of CHAR ([Fig. 3](#)). The increase in CHAR values is likely related to the increased woody species biomass within the landscape at this time, as indicated by the increase in montane forest and the PAR ([Fig. 3](#), Supplementary Fig. 1). At 8200 cal BP, we see a large increase in charcoal counts, decreasing at the very top of the core around ~6800 cal BP. The large increase in charcoal during this period could reflect a regional increase in burning during this time ([Williams et al., 2015](#)) and is likely also representative of a change in vegetation structure, with more available biomass to burn with an increase in heath and tree species, such as Rhamanaceae (*Pomaderris*) and a decrease in the abundance of grasses ([Fig. 3](#) and Supplementary Fig. 1).

The increase in temperature and moisture suggested by pollen is further indicated by an increase in organic matter (OM). From 13,000 cal BP, OM percentages increased sharply (5.4% $\pm$ 2.5 before 13,000 compared to 24.3% $\pm$ 5.2 after 13,000), concurrent with a rise in temperature ([Parrenin et al. 2013](#)) in this period ([Fig. 3](#), Supplementary Table 5). The C:N ratio from 11,700 to 6750 cal BP increases subtly (C:N = 11 to 13.5). We posit this increase in C:N is likely driven partly by an expansion of vegetation cover in the lake catchment, supported by the pollen record ([Fig. 3](#)), increasing more structural C compounds like cellulose and lignin to the lake ([Kaushal and Binford, 1999](#)).

3.4. Mercury concentration and accumulation rate

Mercury concentrations (Hg$_C$) in Blue Lake ranged from 9.8 to 72.9 ng g^{-1}, averaging 41.6 ($\pm$ 18.5) across the core. The lowest Hg$_C$ were recorded in the Pleistocene ([Fig. 3](#), [Table 1](#)), followed by moderate Hg$_C$ in the Holocene transition, and the highest Hg$_C$ in the early Holocene ([Fig. 3](#), [Table 1](#), Supplementary Table 5).

Mercury accumulation rates (Hg$_{AR}$) ranged from 1.2 to 20.9 (µg m^{-2} yr^{-1}) averaging 7.1 ($\pm$ 4.7) across the core, following similar patterns to Hg$_C$, with lower averages in the Pleistocene and Holocene transition compared with the early Holocene ([Table 1](#), Supplementary Table 5, [Fig. 3](#)).

Organic matter and Hg$_c$ and Hg$_{AR}$ are highly correlated (R$_{Pearson}$ = 0.94 and 0.78 respectively, Supplementary Fig. 2) as Hg$_C$ increases, so does OM. When Hg$_C$ is normalised to OM, after 18,000 Cal BP, there are no significant observable changes in the Hg$_c$/OM record ([Fig. 4](#)). Terrestrial organic matter is known to be a large contributor of Hg into lakes ([Hermanns et al., 2013](#)). The increase in Hg in Blue Lake is therefore likely linked to OM export from the catchment.

3.4.1. Pleistocene

Mercury results (Hg$_C$ and Hg$_{AR}$) fluctuate from the base of the core to 18,000 cal BP. Due to the extrapolated age depth model and lack of C:N

Table 1

Mean mercury concentration (Hg$_C$), Hg accumulation rate (Hg$_{AR}$) in sediments of Blue Lake, and Antarctic temperature ([Parrenin et al. 2013](#)) grouped by each period for this study. Due to uncertainty in the sedimentation rate at the base of the core (part of the Pleistocene), HgAR values for this section should be viewed with caution. For *p*-values see Supplementary Table 7.

	Hg$_C$ (ng g^{-1})	Hg$_{AR}$ (µg m^{-2} yr^{-1})	Temperature (°C)
Pleistocene termination	19.4 ($\pm$ 7.1)	3.1 ($\pm$ 1.7)	−6.7 ($\pm$ 2.0)
Holocene transition	29.3($\pm$ 9.9)	3.1 ($\pm$ 1.4)	−2.1 ($\pm$ 0.9)
Early Holocene	56.5($\pm$ 6.9)	10.3($\pm$ 3.8)	0.39($\pm$ 0.47)

data at the base of the core, it is difficult to contextualise the peaks in Hg during this period. The increase in Hg during this period could have been caused by high winds ([Pérez-Rodríguez et al., 2018](#)); the Hg fluctuations overlap with the presence of far-travelled pollen from species occurring outside of the alpine region. However, it is possible that the prevalence of these pollen taxa was primarily due to a lack of local vegetation ([Fig. 3](#)). There is evidence to suggest that the end of the Pleistocene was a windy period in other parts of Australia ([Williams et al., 2001](#); [Stanley and De Deckker, 2002](#); [Hesse and McTainsh, 2003](#); [Petherick et al., 2009](#)).

For the part of the Blue Lake core where the age-depth model was not extrapolated (< 18,000 cal BP), the Hg record encompassing both Hg$_C$ and Hg$_{AR}$ presents an increasing trend with climatic changes recorded in Antarctica (temperature), and the Australian Alps bioregion ([Fig. 3](#); [Parrenin et al. 2013](#)). The escalation of Hg in the Blue Lake sediment sequence initiates around 17,000 cal BP and experiences a notable stabilisation at approximately 15,000 cal BP, corresponding to the period known as the Antarctic Cold Reversal (ACR) ([Pedro et al., 2016](#)). The extent to which the ACR impacted South-Eastern Australia is not well known ([Pedro et al., 2016](#)), but recent analysis has suggested its influence on Australian environments was more widespread than previously suggested ([Cadd et al., 2024](#)). Another recent study, aimed at reconstructing climatic deglacial and Holocene change in the Australian Alps bioregion using paleoenvironmental records from Blue Lake, found evidence to suggest that the ACR occurred around 14,900 to 12,600 cal BP in Blue Lake ([Burdick, 2022](#)). The study of [Burdick (2022)](#) used a combination of OM %, grain size, Si/Ti, Zr, Rb, magnetic susceptibility and visual inspections of the sediment to conclude that the catchment had only a small amount of local vegetation with sediment deposition coming from the catchment and aeolian dust. The lack of vegetation indicated a cold and likely dry environment, indicating that the ACR influenced the environments in the Australian Alpine bioregion. Our findings – that Hg increase was interrupted during the ACR ([Fig. 3](#)) – add to the interpretations of [Burdick (2022)](#) of a cold and dry environment and suggest the ACR was an important climatic event in the Australian Alps bioregion of Australia ([Cadd et al., 2024](#)). Importantly, they show the close link between temperature and precipitation to Hg deposition in the lake.

3.4.2. Onset of the Holocene

The most significant increase in Hg within the Blue Lake profile occurs at the onset of the Holocene, approximately 12,000 cal BP ([Fig. 3](#)). This increase coincides with a vegetation shift from heath-dominated to tree- and swamp-dominated communities and a significant increase in OM and C:N in the lake. These changes in vegetation composition, along with increasing fire activity, collectively indicate a transition towards a warmer and wetter epoch.

With the onset of the Holocene, Hg$_C$ normalised to OM ([Fig. 4](#)) decline and stabilise. The concurrent increases in C:N ratios and OM during the Holocene suggest that the rise in Hg in Blue Lake is likely due to soil development and nutrient input in the catchment area ([Hermanns et al., 2013](#); [Heckmann et al., 2016](#)), which was likely rocky, relatively barren, and covered with ice and snow. As soils and terrestrial vegetation developed, the supply of OM and Hg to the lake increased. While soil development in Blue Lake was likely climate induced, as a result of warming and increased precipitation, the increase in Hg in the lake is only indirectly related to temperature changes and/or increase in atmospheric Hg fallout, potentially masked by local catchment input.

A distinct peak in Hg$_{AR}$ is noted in the uppermost section of the core, ranging between 8000 and 7000 cal BP ([Fig. 3](#)). This peak does not appear to signify an authentic increase in Hg$_{AR}$; instead, it appears to be an artifact resulting from an elevated sedimentation rate. This section of the core had three radiocarbon dates close together (415 cm, 419 cm, and 426 cm) constraining the age model by radiocarbon probability distributions, we posit that this increase in sedimentation rate is therefore likely an artifact of the age-depth model. Notably, Hg$_C$ does not
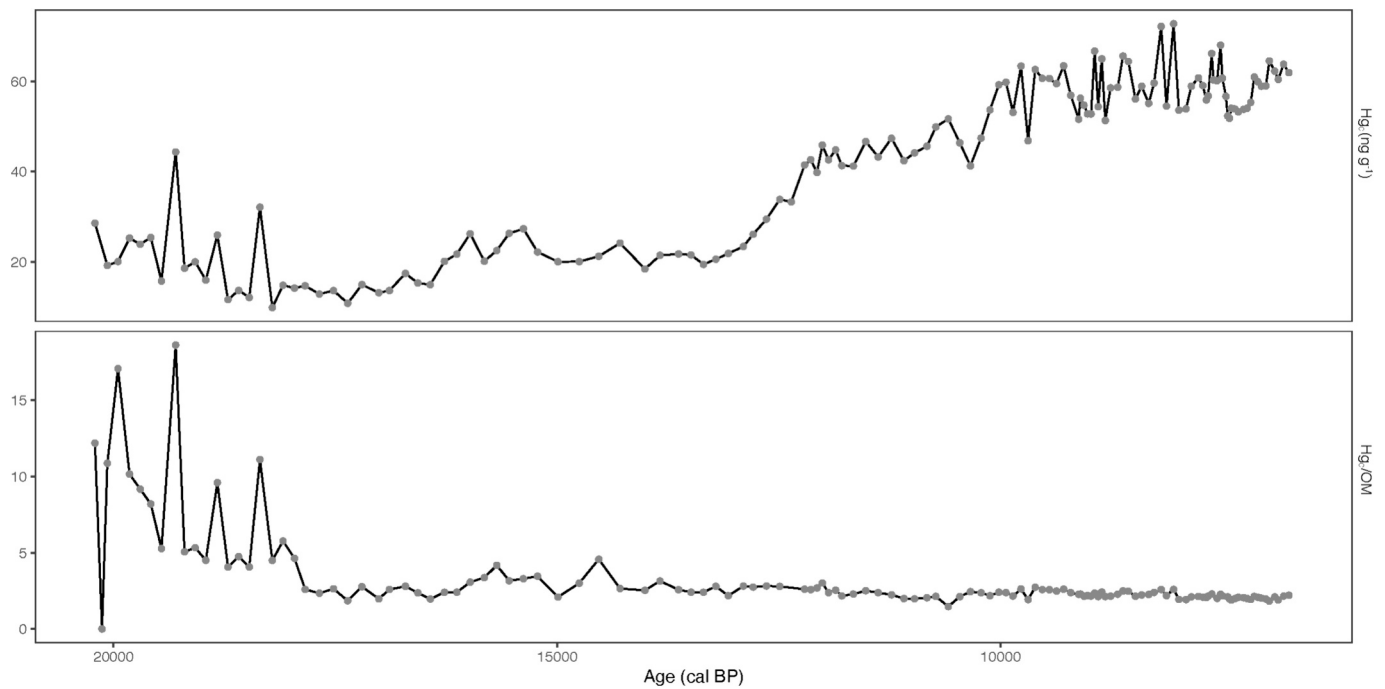
Fig. 4. Stratigraphic diagram of mercury concentration = Hg$_c$ (ng g^{-1}), and mercury concentration divided by organic matter = Hg$_c$/OM. Solid black lines indicate the trend in the data, grey points indicate measured values.

exhibit a peak alongside Hg$_{AR}$ during this brief period.

3.4.3. Possible sources of mercury to Blue Lake, as indicated by the climate proxies

Multivariate ordination of the terrestrial pollen data shows a clear separation between time periods (DCA, Fig. 5a, (See Supplementary Table 6 for terrestrial pollen included in the DCA)). Axis 1 of the DCA, when plotted against age (Fig. 5b), correlates with the deglacial temperatures observed in both the Antarctic ice core temperature data (Supplementary Fig. 3, $R = 0.76$), and the modelled temperature data in the Blue Lake region (Fig. 3). The three top positive taxa associated with axis 1 (early Holocene samples on the right-hand side of Fig. 5a), are *Epacris* (heath, found in moist/wet environments), *Eucalyptus viminalis*-type (representing trees) and Apiaceae (herbs often found in alpine environments), indicating a warm and wet environment similar to the present-day. The three top negative taxa associated with axis 1 (late Pleistocene samples on the left-hand side of Fig. 5a), are *Plantago*, Asteraceae, and Amaranthaceae, all herbs associated with dry or variable environments (Supplementary Table 6).

Further to the DCA analyses, a multi-proxy PCA reflects the changes in climate within the core (Fig. 6). Axis 1 explains 69% of the variation in the data with negative weights on PC1 for high temperatures, high organic matter, high C:N ratio and pollen taxa associated with wetter and warmer climates (indicated by higher values on DCA axis 1 plotted within the PCA, Supplementary Table 6), suggesting a climate driver for this axis. Mercury accumulation rate is plotted passively, with the highest values also weighted negatively on PC1, indicating that higher temperature, C:N ratios, and OM are the main drivers of Hg$_{AR}$ in Blue Lake (Fig. 6). Time periods are separated along the PC1 axis, with the Pleistocene Termination on the positive end (colder climate), and the early Holocene, slightly negatively (warmer climate) (Fig. 6). The separation of proxies and time periods along PC1 indicates that Hg$_{AR}$ is being influenced by climatic factors, with warmer and wetter environments leading to an increase in Hg$_{AR}$. However, due to Hg's close correlation with OM, changes in temperature and precipitation are likely only indirectly increasing Hg in the lake sediments. Instead, the OM results suggest that the warmer and wetter climate in the Holocene

facilitated soil and vegetation development, enhancing Hg accumulation in the lake catchment through plant uptake and binding to soil OM, the two main mechanisms of Hg fluxes from the atmosphere to terrestrial ecosystems (for examples see: Guédron et al., 2018; Bishop et al., 2020; Gómez-Armesto et al., 2020; Zhou et al., 2021, 2023). Thus, erosion and transport of newly developed soils from the glacial catchment into the lake may have enhanced Hg fluxes to the lake. Potential changes from atmospheric Hg fallout are likely overshadowed by the inputs of Hg bound to organic matter in the lake (Fig. 4).

The PC2 axis explains 20% of the variation in the data. The CHAR is strongly positively weighted on PC2, and not located near any other climate proxy, suggesting that variations in fire activity have occurred out of step, or variability in association with the climatic variables. Mercury is unrelated to PCA axis 2, giving further evidence to support our hypothesis that Hg deposition in Blue Lake was primarily driven by local changes in the catchment, which have evolved in response to climate changes.

The effects of climate change on Hg$_{AR}$ are a result of more than one environmental variable and ecological process, such as precipitation, winds, vegetation changes, soil development, and not a result of a singular climate factor (Martinez-Cortizas et al., 1999; Biester et al., 2007; Driscoll et al., 2013). In Blue Lake, the relationship between rising temperatures, increased precipitation, C:N, and OM indicate that Hg$_C$ and Hg$_{AR}$ are likely indirectly driven by climate warming, via an increase in vegetation biomass in the catchment, development of soil after deglaciation and organic matter associated with Hg inputs to the lake.

3.4.4. 4- past climate Variability and Mercury Shifts: Implications for Environmental policies in the Anthropocene

The synthesis of sediment records, climate proxy data, and Hg$_{AR}$ offers a comprehensive understanding of how climate-induced, and local modifications can impact various processes within the Hg cycle in ecosystems. Given Hg's sensitivity to physical transformations, especially to changes in organic matter inputs, investigating its historical response to known climate variations and land transformations is crucial for predicting future Hg exposure in the context of the Anthropocene.

Despite a significant body of Hg research conducted in the last two
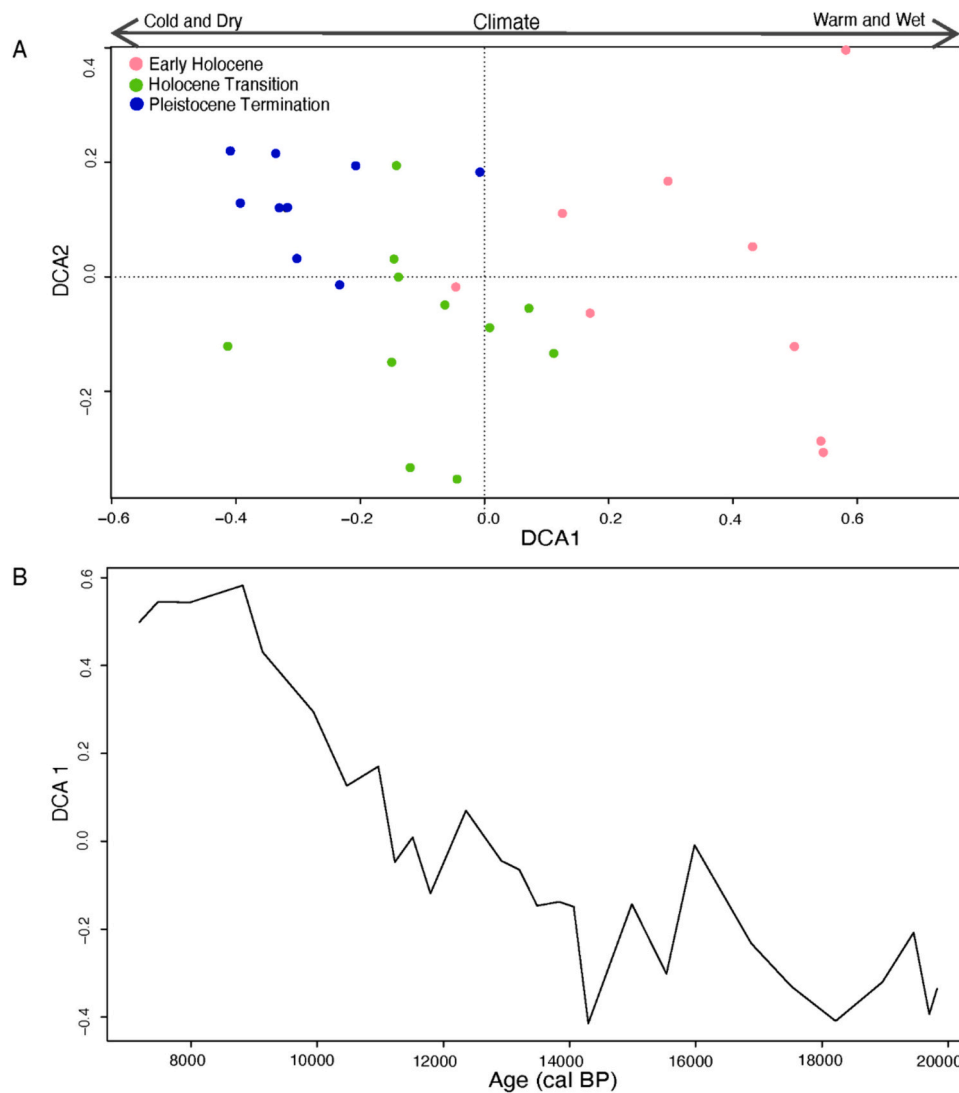
Fig. 5. Detrended correspondence analysis (DCA) of the terrestrial pollen record from Blue Lake. Site level DCA (A) with time periods indicated by coloured dots, pink = Early Holocene, green = Holocene Transition, and blue = Pleistocene Termination. Axis 1 of DCA represented in panel A plotted against Age (B). (For interpretation of the references to colour in this figure legend, the reader is referred to the web version of this article.)

decades, one of the primary challenges among the Hg research and policy communities is disentangling changes in Hg attributable to anthropogenic activities from those caused by climate change. Palaeo records provide a unique opportunity for distinct analyses of natural Hg responses to climate, and disturbance-driven changes (Cooke et al., 2020).

Forecasts for the alpine region of Australia predict an anticipated rise in mean annual temperature by 2050, ranging from 0.6 to 2.6 °C, and up to 4.5 °C by 2100 (Hennessy et al., 2008; Thomas et al., 2022). Studies on the effect of climate factors on soil have demonstrated an elevated risk of soil erosion due to global warming (Brazier et al., 2000; Zhao et al., 2022; Li and Fang, 2016). Our results revealed that Hg deposition in Blue Lake increased during warm phases and was primarily driven by OM inputs from the catchment. The evidence linking soil erosion to climate change and our findings on Hg increases with the onset of the Holocene underscore the importance of considering climate warming and the risk of land disturbance in policy adjustments aimed at mitigating Hg increases in lakes. Notably, our study demonstrates that a 4.3 °C rise in temperature, associated with climate changes, soil and vegetation dynamics, resulted in a threefold increase in Hg in Blue Lake (Fig. 3), between approximately 14,000 cal BP (8.7 °C, Hg_{AR} = 1.49 ng $m^{-2} y^{-1}$) and approximately 11,500 cal BP (13 °C, Hg_{AR} = 5.19 ng m^{-2}

y^{-1}).

Rapid climate warming and the consequent increase in soil fluxes from the lake catchment, can significantly elevate Hg deposition in Australian alpine ecosystems. Thomas et al., (2022) also found increased Hg deposition in Club Lake (located only 3 km from Blue Lake), as a result of a warming climate. Our findings indicate that climate warming should be considered in regulatory frameworks aimed at reducing Hg pollution in aquatic environments.

4. Conclusions

The Blue Lake sediment geochemistry and pollen record presented in this study provides important quantitative data on the climate of Australia's alpine region towards the end of the Pleistocene into the early Holocene. Our pollen and geochemistry results suggest a dry and cold Pleistocene termination and a warm and wet early Holocene. Our study provides further evidence that Hg is a useful proxy for understanding environmental change, with the potential to improve our understanding of past climatic changes in South-Eastern Australia. Mercury accumulation rates tripled with a 4.3 °C temperature increase from the Pleistocene to Holocene, mainly driven by OM and increased nutrient transport from the catchment. A maximum risk projection of a 4.5 °C
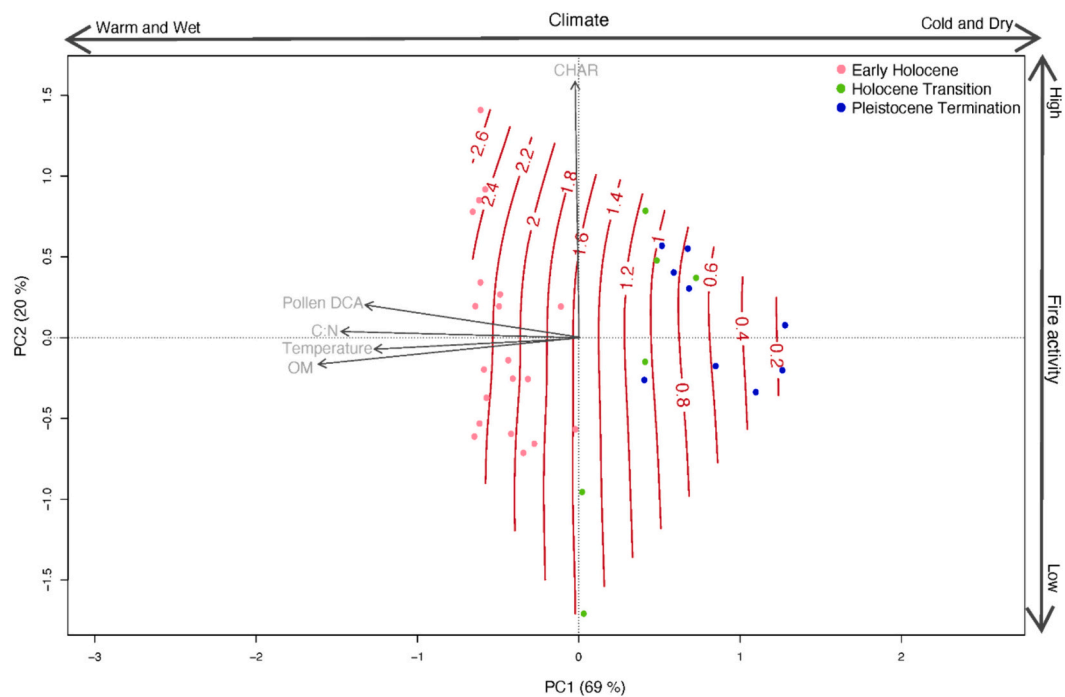
Fig. 6. Principal components analysis (PCA) of the multiproxy profile of Blue Lake. PC1 and PC2 explain 69% and 20% of the variation respectively, total explained = 89%. Pink dots = early Holocene samples, green dots = Holocene transition samples, blue dots = Pleistocene samples. Orange lines indicate log-transformed mercury accumulation rate (ng m^{-2} y^{-1}), C:N = carbon:nitrogen ratio log-transformed, Temperature = reconstructed Antarctic temperature (Parrenin et al., (2013)) + 10 and log transformed, OM=Organic matter log-transformed, pollen DCA = extrapolated data from Axis 1 of the pollen DCA (Fig. 5). PC1 indicates a climate trend, with negative values = warm and wet environments, and positive = cold and dry. PC2 indicates fire activity, positive PC2 = high fire activity, negative PC2 = low fire activity. (For interpretation of the references to colour in this figure legend, the reader is referred to the web version of this article.)

increase in the Australian Alps bioregion has been modelled (1 to 4.5 °C) by 2100, in combination with increased risk of soil erosion with increasing temperatures, suggests current rates of Hg$_{AR}$ could rapidly increase with global warming. Both direct and indirect pathways of Hg$_{AR}$ need to be considered in future research. By furthering our knowledge of how Southern Hemisphere Hg$_{AR}$ has responded to past change, we can continue to refine the use of Hg in combination with other proxies to disentangle past climatic events and predict future change. With such large projected temperature increases, these findings highlight the importance of considering climate change in policy adjustments aimed at reducing Hg pollution in aquatic environments.

CRediT authorship contribution statement

Margot Aurel Schneider: Writing – original draft, Visualization, Methodology, Investigation, Formal analysis, Data curation. **Larissa Schneider:** Writing – original draft, Visualization, Methodology, Investigation, Funding acquisition, Formal analysis, Conceptualization. **Haidee Cadd:** Writing – original draft, Methodology, Investigation, Formal analysis, Data curation. **Zoë A. Thomas:** Writing – original draft, Visualization, Formal analysis, Data curation, Conceptualization. **Antonio Martinez-Cortizas:** Writing – original draft, Investigation. **Simon Edward Connor:** Writing – original draft, Formal analysis. **Georgia L. Stannard:** Writing – original draft, Data curation. **Simon Graeme Haberle:** Writing – original draft, Conceptualization.

Declaration of competing interest

The authors declare that they have no known competing financial interests or personal relationships that could have appeared to influence the work reported in this paper.

Data availability

Pollen data will be available via Neotoma.

Acknowledgments

Appendix A. Supplementary data

Supplementary data to this article can be found online at https://doi.org/10.1016/j.gloplacha.2024.104539.

References

Auld, J., Everingham, S.E., Hemmings, F.A., Moles, A.T., 2022. Alpine plants are on the move: Quantifying distribution shifts of Australian alpine plants through time. Divers. Distrib. 28 (5), 943–955. https://doi.org/10.1111/ddi.13494.

Barrows, T.T., Stone, J.O., Fifield, L.K., Cresswell, R.G., 2001. Late Pleistocene Glaciation of the Kosciuszko Massif, Snowy Mountains, Australia. Quat. Res. 55 (2), 179–189. https://doi.org/10.1006/qres.2001.2216.

Beckers, F., Rinklebe, J., 2017. Cycling of mercury in the environment: sources, fate, and human health implications: A review. Crit. Rev. Environ. Sci. Technol. 47 (9), 693–794.

Biester, H., Bindler, R., Martinez-Cortizas, A., Engstrom, D.R., 2007. Modeling the Past Atmospheric Deposition of Mercury using Natural Archives. Environ. Sci. Technol. 41 (14), 4851–4860. https://doi.org/10.1021/es0704232.

Bishop, K., Shanley, J., Riscassi, A., de Wit, H., Eklöf, K., Meng, B., Mitchell, C., Osterwalder, S., Schuster, P., Webster, J., Zhu, W., 2020. Recent advances in understanding and measurement of mercury in the environment: Terrestrial Hg

cycling. Sci. Total Environ. 721, 137647 https://doi.org/10.1016/j. scitotenv.2020.137647.

Brady, E., Stevenson, S., Bailey, D., Liu, Z., Noone, D., Nusbaumer, J., Otto-Bliesner, B.L., Tabor, C., Tomas, R., Wong, T., Zhang, J., Zhu, J., 2019. The Connected Isotopic Water Cycle in the Community Earth System Model Version 1. Journal of Advances in Modeling Earth Systems 11 (8), 2547–2566. https://doi.org/10.1029/ 2019MS001663.

Brazier, R.E., Beven, K.J., Freer, J., Rowan, J.S., 2000. Equifinality and uncertainty in physically based soil erosion models: application of the GLUE methodology to WEPP–the Water Erosion Prediction Project–for sites in the UK and USA. Earth Surf. Process. Landf. 25 (8), 825–845. https://doi.org/10.1002/1096-9837(200008)25: 8<825::AID-ESP101>3.0.CO;2-3.

Bronk Ramsey, C., 2008. Radiocarbon Dating: Revolutions in Understanding*. Archaeometry 50 (2), 249–275. https://doi.org/10.1111/j.1475-4754.2008.00394. x.

Burdick, A.W., 2022. Reconstructing Deglacial and Holocene Climatic and Environmental Change in the Snowy Mountains of Southeast Australia.

Cadd, H., Petherick, L., Tyler, J., Herbert, A., Cohen, J.T., Sniderman, K., Barrows, T.T., Fulop, H.R., Knight, J., Kershaw, A.P., Colhoun, A.E., Harris, R.P.M., 2021. A continental perspective on the timing of environmental change during the last glacial stage in Australia. Quat. Res. 102, 5–23. https://doi.org/10.1017/ qua.2021.16.

Cadd, H., Saktura, W., Cohen, T., Mooney, S., He, C., Turney, C.S.M., Otto-Bliesner, B., 2024. Last Glacial Maximum cooling induced positive moisture balance and maintained stable human populations in Australia. Communications Earth & 5, 52. https://doi.org/10.1038/s43247-024-01204-1.

Cooke, C.A., Martínez-Cortizas, A., Bindler, R., Sexauer Gustin, M., 2020. Environmental archives of atmospheric Hg deposition - A review. Sci. Total Environ. 709, 134800 https://doi.org/10.1016/j.scitotenv.2019.134800.

Cooke, C.A., Curtis, J.H., Kenney, W.F., Drevnick, P., Siegel, P.E., 2022. Caribbean Lead and Mercury Pollution Archived in a Crater Lake. Environ. Sci. Technol. 56 (3), 1736–1742. https://doi.org/10.1021/acs.est.1c06791.

Costin, A.B., Gray, M., Totterdell, C.J., Wimbush, D.J., 1979. Kosciusko alpine flora. Brunonia 2 (2), 321–322.

David, S.T.W.E., Helms, R., Pittman, E.F., 1901. Geological Notes on Kosciusko: With Special Reference to Evidences of Glacial Action.

De Deckker, P., Van Der Kaars, S., Macphail, M.K., Hope, G.S., 2019. Land-sea correlations in the Australian region: 460 ka of changes recorded in a deep-sea core offshore Tasmania. Part 1: the pollen record. Aust. J. Earth Sci. 66 (1), 1–15. https:// doi.org/10.1080/08120099.2018.1495100.

De Deckker, P., Moros, M., Perner, K., Blanz, T., Wacker, L., Schneider, R., Barrows, T.T., O'loingsigh, T., Jansen, E., 2020. Climatic evolution in the Australian region over the last 94 ka-spanning human occupancy-, and unveiling the last Glacial Maximum. Quat. Sci. Rev. 249, 106593.

De Deckker, P., Hancock, G.J., Olley, J.M., Stanley, S., Hope, G., 2023. The effect of the introduction of livestock on the erosion of alpine soils: a comparison of five dating techniques applied to sediments of the Australian alpine Blue Lake. J. Paleolimnol. 70 (2), 77–93. https://doi.org/10.1007/s10933-023-00284-x.

Devesa-Rey, R., Barral, M.T., 2012. Allochthonous versus autochthonous naturally occurring organic matter in the Anllóns river bed sediments (Spain). Environ. Earth Sci. 66 (3), 773–782. https://doi.org/10.1007/s12665-011-1286-3.

Driscoll, C.T., Mason, R.P., Chan, H.M., Jacob, D.J., Pirrone, N., 2013. Mercury as a Global Pollutant: sources, Pathways, and Effects. Environ. Sci. Technol. 47 (10), 4967–4983. https://doi.org/10.1021/es305071v.

Du, Y., Brown, J.R., Sniderman, J.K., 2023. Last Glacial Maximum climate and Atmospheric Circulation over the Australian Region from climate Models. Clim. Past Discuss. 2023, 1–34.

Dulhunty, J.A., 1945. On glacial lakes in the Kosciusko region, pp. 143–152.

Engstrom, D.R., Fitzgerald, W., Cook, A.C., Lamborg, H.C., Drevnick, E.P., Swain, B.E., Balogh, J.S., Balcom, H.P., 2014. Atmospheric Hg emissions from preindustrial gold and silver extraction in the Americas: A reevaluation from lake-sediment archives. Environ. Sci. Technol. 48 (12), 6533–6543.

Faegri, K., Kaland, P.E., Krzywinski, K., 1989. Textbook of Pollen Analysis. John Wiley & Sons Ltd.

Fitzgerald, W., Lamborg, C., 2005. Geochemistry of Mercury. Environmental Geochemistry 9, 107.

Fitzgerald, W.F., Engstrom, D.R., Hammerschmidt, R.C., Lamborg, H.C., Balcom, H.P., Lima-Braun, L.A., Bothner, H.M., Reddy, M.C., 2018. Global and local sources of mercury deposition in coastal New England reconstructed from a multiproxy, high-resolution, estuarine sediment record. Environ. Sci. Technol. 52 (14), 7614–7620.

Gómez-Armesto, A., Méndez-López, M., Pérez-Rodríguez, P., Fernández-Calviño, D., Arias-Estévez, M., Nóvoa-Muñoz, J.C., 2020. Litterfall Hg deposition to an oak forest soil from southwestern Europe. J. Environ. Manag. 269, 110858 https://doi.org/ 10.1016/j.jenvman.2020.110858.

Green, K., Pickering, C.M., 2009. The decline of snowpatches in the Snowy Mountains of Australia: importance of climate warming, variable snow, and wind. Arct. Antarct. Alp. Res. 41 (2), 212–218.

Guédron, S., et al., 2018. Mercury Isotopic Fractionation during Pedogenesis in a Tropical Forest Soil Catena (French Guiana): Deciphering the Impact of Historical Gold Mining. Environ. Sci. Technol. 52 (20), 11573–11582. https://doi.org/ 10.1021/acs.est.8b02186.

He, C., Liu, Z., Otto-Bliesner, L.B., Brady, C.E., Zhu, C., Tomas, R., Buizert, C., Severinghaus, P.J., 2021a. Abrupt Heinrich Stadial 1 cooling missing in Greenland oxygen isotopes. Sci. Adv. 7 (25), eabh1007. https://doi.org/10.1126/sciadv. abh1007.

He, C., Liu, Z., Otto-Bliesner, L.B., Brady, C.E., Zhu, C., Tomas, R., Gu, S., Han, J., Jin, Y., 2021b. Deglacial variability of South China hydroclimate heavily contributed by autumn rainfall. Nat. Commun. 12 (1), 5875. https://doi.org/10.1038/s41467-021- 26106-0.

Heckmann, T., McColl, S., Morche, D., 2016. Retreating ice: research in pro-glacial areas matters. Earth Surf. Process. Landf. 41 (2), 271–276. https://doi.org/10.1002/ esp.3858.

Hennessy, K.J., Whetton, P.H., Walsh, K., Smith, I.N., Bathols, J.M., Hutchinson, M., Sharples, J., 2008. Climate change effects on snow conditions in mainland Australia and adaptation at ski resorts through snowmaking. Clim. Res. 35 (3), 255–270. https://doi.org/10.3354/cr00706.

Hermanns, Y.-M., Biester, H., 2013. A 17,300-year record of mercury accumulation in a pristine lake in southern Chile. J. Paleolimnol. 49 (4), 547–561. https://doi.org/ 10.1007/s10933-012-9668-4.

Hermanns, Y.-M., Cortizas, A.M., Arz, H., Stein, R., Biester, H., 2013. Untangling the influence of in-Lake productivity and terrestrial organic matter flux on 4,250 years of mercury accumulation in Lake Hambre, Southern Chile. J. Paleolimnol. 49 (4), 563–573. https://doi.org/10.1007/s10933-012-9657-7.

Hesse, P.P., McTainsh, G.H., 2003. Australian dust deposits: modern processes and the Quaternary record. Quat. Sci. Rev. 22 (18), 2007–2035. https://doi.org/10.1016/ S0277-3791(03)00164-1.

Hogg, A.G., Heaton, J.T., Hua, Q., Palmer, S.M.C., Turney, S.M.C., Southon, J., Bayliss, A., Blackwell, G.P., Boswijk, G., Ramsey, B., Pearson, C., Petchey, F., Reimer, P., Reimer, R., Wacker, L., 2020. SHCal20 Southern Hemisphere Calibration, 0–55,000 years cal BP. Radiocarbon 62 (4), 759–778. https://doi.org/10.1017/ RDC.2020.59.

Kassambara, A., Kassambara, M.A., 2020. Package 'ggpubr.' R package version 0.1 6(0).

Kaufman, D.S., Broadman, E., 2023. Revisiting the Holocene global temperature conundrum. Nature 614 (7948), 425–435. https://doi.org/10.1038/s41586-022- 05536-w.

Kaushal, S., Binford, M.W., 1999. Relationship between C: N ratios of Lake sediments, organic matter sources, and historical deforestation in Lake Pleasant, Massachusetts, USA. J. Paleolimnol. 22, 439–442.

Kershaw, A.P., Clark, J.S., Gill, A.M., D'COSTA, D.M., 2002. A History of Fire in Australia.

Kessler, R., 2013. The Minamata Convention on Mercury: A First Step toward Protecting Future Generations.

Kessler, M., Kluge, J., 2022. Mountain Ferns: what Determines their Elevational Ranges and how will they Respond to climate Change? American Fern Journal 112 (4), 285–302. https://doi.org/10.1640/0002-8444-112.4.285.

Lamborg, C., Fitzgerald, W., Damman, A., Benoit, J., Balcom, P., Engstrom, D., 2002. Modern and historic atmospheric mercury fluxes in both hemispheres: global and regional mercury cycling implications. Glob. Biogeochem. Cycles 16 (4), 51.

Leaney, F.W.J., Allison, G.B., Dighton, J.C., Trumbore, S., 1995. The age and hydrological history of Blue Lake, South Australia. Palaeogeogr. Palaeoclimatol. Palaeoecol. 118 (1), 111–130. https://doi.org/10.1016/0031-0182(94)00133-S.

Li, Z., Fang, H., 2016. Impacts of climate change on water erosion: A review. Earth Sci. Rev. 163, 94–117. https://doi.org/10.1016/j.earscirev.2016.10.004.

Li, C., Sonke, E.J., Le Roux, G., Piotrowska, N., Van der Putten, N., Roberts, J.S., Daley, T., Rice, E., Gehrels, R., Enrico, M., Mauquoy, D., Roland, P.T., De Vleeschouwer, F., 2020. Unequal Anthropogenic Enrichment of Mercury in Earth's Northern and Southern Hemispheres. ACS Earth and Space Chemistry 4 (11), 2073–2081. https://doi.org/10.1021/acsearthspacechem.0c00220.

Lin, C.-J., Pehkonen, S.O., 1999. The chemistry of atmospheric mercury: a review. Atmos. Environ. 33 (13), 2067–2079. https://doi.org/10.1016/S1352-2310(98) 00387-2.

Lindberg, S., Bullock, R., Ebinghaus, R., Engstrom, D., Feng, X., Fitzgerald, W., Pirrone, N., Prestbo, E., Seigneur, C., 2007. A synthesis of progress and uncertainties in attributing the sources of mercury in deposition. AMBIO: a Journal of the Human Environment 36 (1), 19–33.

Linder, H.P., Briggs, B.G. and Johnson, L.A.S. 1998. Restionaceae. In: Kubitzki, K. ed. Flowering Plants · Monocotyledons: Alismatanae and Commelinanae (except Gramineae). The Families and Genera of Vascular Plants. Berlin, Heidelberg: Springer, Pp. 425–445. Available at: https://doi.org/10.1007/978-3-662-0 3531-3_41 [Accessed: 16 January 2024].

Long, K.E., Schneider, L., Connor, E.S., Shulmeister, N., Finn, J., Roberts, L.G., Zawadki, A., Enge, G.T., Smol, P.J., Ballard, C., 2021. Human impacts and Anthropocene environmental change at Lake Kutubu, a Ramsar wetland in Papua New Guinea. Proc. Natl. Acad. Sci. 118 (40), e2022216118.

Mackereth, F.J.H., 1958. A Portable Core Sampler for Lake Deposits. Limnol. Oceanogr. 3 (2), 181–191. https://doi.org/10.4319/lo.1958.3.2.0181.

Mariani, M., Beck, K.K., Fletcher, M.-S., Gell, P., Saunders, K.M., Gadd, P., Chisari, R., 2018. Biogeochemical responses to Holocene Catchment-Lake Dynamics in the Tasmanian World Heritage Area. Australia. Journal of Geophysical Research: Biogeosciences 123 (5), 1610–1624. https://doi.org/10.1029/2017JG004136.

Martin, A.R.H., 1999. Pollen Analysis of Digger's Creek Bog, Kosciuszko National Park: Vegetation history and Tree-line Change. Aust. J. Bot. 47 (5), 725–744. https://doi. org/10.1071/bt98002.

Martinez-Cortizas, A., Pontevedra-Pombal, X., Garcia-Rodeja, E., Novoa-Munoz, J.C., Shotyk, W., 1999. Mercury in a Spanish Peat Bog: Archive of Climate Change and Atmospheric Metal Deposition. Science (New York, N.Y.) vol. 284 (5416), 939–942. https://doi.org/10.1126/science.284.5416.939.

Menviel, L., Spence, P., Yu, J., Chamberlain, M., Matear, R., Meissner, K., England, M.H., 2018. Southern Hemisphere westerlies as a driver of the early deglacial atmospheric CO2 rise. Nat. Commun. 9 (1), 2503.

Obrist, D., Kirk, J.L., Zhang, L., Sunderland, E.M., Jiskra, M., Selin, N.E., 2018. A review of global environmental mercury processes in response to human and natural perturbations: changes of emissions, climate, and land use. Ambio 47 (2), 116–140. https://doi.org/10.1007/s13280-017-1004-9.

Oksanen, J., 2015. Vegan: An Introduction to Ordination.

Oksanen, J., Kindt, R., Legendre, P., O'Hara, B., Stevens, M.H.H., Oksanen, M.J., Suggests, M., 2007. The vegan package. Community ecology package 10 (631–637), 719.

Orchard, A., 1979. Myriophyllum (Haloragaceae) in Australasia. 1. New Zealand: A revision of the genus and a synopsis of the family. Brunonia 2 (2), 247–287.

Outridge, P.M., Mason, R.P., Wang, F., Guerrero, S., Heimbürger-Boavida, L.E., 2018. Updated Global and Oceanic Mercury Budgets for the United Nations Global Mercury Assessment 2018. Environ. Sci. Technol. 52 (20), 11466–11477. https://doi.org/10.1021/acs.est.8b01246.

Parrenin, F., Masson-Delmotte, V., Köhler, P., Raynaud, D., Paillard, D., Schwander, J., Barbante, C., Landais, A., Wegner, A., Jouzel, J., 2013. Antarctic Temperature Stack (ATS) from five different ice cores (EDC, Vostok, Dome Fuji, TALDICE, and EDML). In supplement to: Parrenin, F et al. (2013): Synchronous change of atmospheric CO2 and Antarctic temperature during the last deglacial warming. Science 339 (6123), 1060–1063. https://doi.org/10.1126/science.1226368. Available at: https://doi.org/10.1594/PANGAEA.810188.

Pedro, J.B., Bostock, C.H., Bitz, M.C., He, F., Vandergoes, J.M, Steig, J.E., Chase, M.B., Krause, E.C., Rasmussen, O.S., Markle, R.B., Cortese, G. 2016. The spatial extent and dynamics of the Antarctic Cold Reversal. Nat. Geosci. 9(1), pp. 51–55. doi:https://doi.org/10.1038/ngeo2580.

Pérez-Rodríguez, M., Margalef, O., Corella, J.P., Saiz-Lopez, A., Pla-Rabes, S., Giralt, S., Martínez Cortizas, A., 2018. The Role of climate: 71 ka of Atmospheric Mercury Deposition in the Southern Hemisphere Recorded by Rano Aroi Mire, Easter Island (Chile). Geosciences 8 (10), 374. https://doi.org/10.3390/geosciences8100374.

Petherick, L.M., McGowan, H.A., Kamber, B.S., 2009. Reconstructing transport pathways for late Quaternary dust from eastern Australia using the composition of trace elements of long traveled dusts. Geomorphology 105 (1), 67–79. https://doi.org/10.1016/j.geomorph.2007.12.015.

Petherick, L.M., Knight, J., Shulmeister, J., Bostock, H., Lorrey, A., Fitchett, J., Eaves, S., Vandergoes, J.M, Barrows, T.T., Barrell, A.J.D., Eze, N.P., Hesse, P., Jara, A.I., Mills, S., Newnham, R., Pedro, J., Ryan, M., Saunders, M.K., White, D., Rojas, M., Turney, C., 2022. An extended last glacial maximum in the Southern Hemisphere: A contribution to the SHeMax project. Earth Sci. Rev. 231, 104090 https://doi.org/10.1016/j.earscirev.2022.104090.

Raine, J.I., 1974. Pollen Sedimentation in Relation to the Quaternary Vegetation History of the Snowy Mountains of New South Wales. The Australian National University (Australia).

Raine, J.I., 1982. Dimictic thermal regime and morphology of Blue Lake in the Snowy Mountains of New South Wales. Mar. Freshw. Res. 33 (6), 1119–1122.

Ramsey, C.B., 2009. Bayesian Analysis of Radiocarbon Dates. Radiocarbon 51 (1), 337–360. https://doi.org/10.1017/S0033822200033865.

Ramsey, C.B., Lee, S., 2013. Recent and Planned Developments of the Program OxCal. Radiocarbon 55 (2), 720–730. https://doi.org/10.1017/S0033822200057878.

Saunders, K.M., Roberts, S.J, Perren, B., Butz, C., Sime, L., Davies, S., Van Nieuwenhuyze, W., Grosjean, M., Hodgson, A.D. 2018. Holocene dynamics of the Southern Hemisphere westerly winds and possible links to CO2 outgassing. Nat. Geosci. 11(9), pp. 650–655. doi:https://doi.org/10.1038/s41561-018-0186-5.

Schneider, L., Cooke, C.A., Stansell, N.D., Haberle, S.G., 2020. Effects of climate variability on mercury deposition during the older Dryas and Younger Dryas in the Venezuelan Andes. J. Paleolimnol. 63 (3), 211–224.

Sigman, D.M., Boyle, E.A., 2000. Glacial/interglacial variations in atmospheric carbon dioxide. Nature 407 (6806), 859–869.

Smith, A.J., 1959. Description of the Mackereth portable core sampler. J. Sediment. Res. 29 (2).

Stanley, S., De Deckker, P., 2002. A Holocene record of allochthonous, aeolian mineral grains in an Australian alpine lake; implications for the history of climate change in southeastern Australia. J. Paleolimnol. 27 (2), 207–219. https://doi.org/10.1023/A:1014249404845.

Stansell, N.D., Rodbell, D.T., Abbott, M.B., Mark, B.G., 2013. Proglacial lake sediment records of Holocene climate change in the western Cordillera of Peru. Quat. Sci. Rev. 70, 1–14. https://doi.org/10.1016/j.quascirev.2013.03.003.

Swartzendruber, P. and Jaffe, D. 2012. 3Sources and Transport: A Global issue. In: Bank, M. ed. *Mercury in the Environment: Pattern and Process*. University of California Press, p. 0. Available at: https://doi.org/10.1525/california/9780520271630.003.0001 [Accessed: 24 January 2024].

Thomas, Z.A., Mooney, S., Cadd, H., Baker, A., Turney, C., Schneider, L., Hogg, A., Haberle, S., Green, K., Weyrick, L.S., Pérez, V., Moore, N.E., Zawadzki, A., Kelloway, S.J., Khan, S.J., 2022. Late Holocene climate anomaly concurrent with fire activity and ecosystem shifts in the eastern Australian Highlands. Sci. Total Environ. 802, 149542 https://doi.org/10.1016/j.scitotenv.2021.149542.

Turney, C., Becerra-Valdivia, L., Sookdeo, A., Thomas, Z.A., Palmer, J., Haines, H>A., Cadd, H.< Wacker, L., Baker, A., Anderson, M.S., Jacobsen, G., Meredith, K., Chnu, K., Bollhalder, S., Marjo, C, 2021. Radiocarbon Protocols and first Intercomparison results from the Chronos 14CARBON-CYCLE Facility, University of New South Wales, Sydney, Australia. Radiocarbon 63 (3), 1003–1023. https://doi.org/10.1017/RDC.2021.23.

UNEP, 2018. Global Mercury Assessment 2018. United Nations Environment Programme, Chemicals and Health Branch, Geneva, Switzerland.

USEPA (US Environmental Protection Agency), 1998. Method 7473: Mercury in solids and solutions by thermal decomposition, amalgamation, and atomic absorption spectrophotometry.

Vernon, J., 2017. Identifying the Impacts of Climate Change and Human Activity in Kosciuszko National Park.

Wang, Q., Li, Y., Wang, Y., 2011. Optimizing the weight loss-on-ignition methodology to quantify organic and carbonate carbon of sediments from diverse sources. Environ. Monit. Assess. 174 (1), 241–257. https://doi.org/10.1007/s10661-010-1454-z.

Wickham, H. and Chang, W. 2016. Package 'ggplot2.' Create elegant data visualisations using the grammar of graphics. Version 2(1), pp. 1–189.

Williams, M., Prescott, J.R., Chappell, J., Adamson, D., Cock, B., Walker, K., Gell, P., 2001. The enigma of a late Pleistocene wetland in the Flinders Ranges, South Australia. Quat. Int. 83–85, 129–144. https://doi.org/10.1016/S1040-6182(01)00035-0.

Williams, M., Cook, E., van der Kaars, S., Barrows, T., Shulmeister, J., Kershaw, P., 2009. Glacial and deglacial climatic patterns in Australia and surrounding regions from 35 000 to 10 000 years ago reconstructed from terrestrial and near-shore proxy data. Quat. Sci. Rev. 28 (23), 2398–2419. https://doi.org/10.1016/j.quascirev.2009.04.020.

Williams, A.N., Mooney, S.D., Sisson, S.A., Marlon, J., 2015. Exploring the relationship between Aboriginal population indices and fire in Australia over the last 20,000years. Palaeogeogr. Palaeoclimatol. Palaeoecol. 432, 49–57. https://doi.org/10.1016/j.palaeo.2015.04.030.

Zhao, J., Wang, Z., Dong, Y., Yang, Z., Govers, G., 2022. How soil erosion and runoff are related to land use, topography and annual precipitation: Insights from a meta-analysis of erosion plots in China. Sci. Total Environ. 802, 149665 https://doi.org/10.1016/j.scitotenv.2021.149665.

Zhou, J., Obrist, D., Dastoor, A., Jiskra, M., Ryjkov, A., 2021. Vegetation uptake of mercury and impacts on global cycling. Nature Reviews Earth & Environment 2 (4), 269–284. https://doi.org/10.1038/s43017-021-00146-y.

Zhou, J., Bollen, S.W., Roy, E.M., Hollinger, D.Y., Wang, T., Lee, J.T., Obrist, D., 2023. Comparing ecosystem gaseous elemental mercury fluxes over a deciduous and coniferous forest. Nat. Commun. 14 (1), 2722. https://doi.org/10.1038/s41467-023-38225-x.